

Aging of the surface of Bi_2Se_3

Deepnarayan Biswas¹, Sangeeta Thakur¹, Khadiza

Ali¹, Geetha Balakrishnan², and Kalobaran Maiti^{1a}

¹*Department of Condensed Matter Physics and Materials' Science,*

Tata Institute of Fundamental Research,

Homi Bhabha Road, Colaba, Mumbai - 400 005, India.

²*Department of Physics, University of Warwick, Coventry, CV4 7AL, UK.*

(Dated: November 5, 2014)

Abstract

We study the electronic structure of Bi_2Se_3 employing high resolution photoemission spectroscopy and discover the dependence of the behavior of Dirac particles on surface terminations. The Dirac cone apex appears at different energies and exhibits contrasting shift on Bi and Se terminated surface with complex time dependence emerging from subtle adsorbed oxygen-surface atom interactions. These results uncover the surface states behavior of real systems possessing topologically ordered surface.

^a Corresponding author: kbmaiti@tifr.res.in

Topological insulators are like ordinary insulators in the bulk with gapless surface states protected by time reversal symmetry [1, 2]. These materials have drawn much attention in the recent times followed by the proposals of the realization of exotic physics involving Majorana Fermions [3], magnetic monopoles [4] etc. In addition to such fundamental interests, the predicted special properties of these states make them useful for the technological applications ranging from spintronics to quantum computations. Although the topological states are protected by time reversal symmetry[5], numerous experiments show instability of the topological states with aging. Plethora of contrasting scenarios, anomaly on absorption of foreign elements, etc. are observed in the experimental studies[5, 6]. It is evident that the real materials are complex and may not be commensurate to the theoretical predictions that makes this issue an outstanding problem in various branches of science and technology.

In order to elucidate these puzzles in real materials, we studied the electronic structure of a typical topological insulator, Bi_2Se_3 at different experimental conditions such as the behavior of differently terminated surface, evolution of the electronic structure on aging, etc. employing high resolution photoemission spectroscopy. Bi_2Se_3 forms in a layered structure (see Fig. 1(a)) with the quintuple layers of Se-Bi-Se-Bi-Se stacked together by Van der Waals force [7]. The surface electronic structure exhibits topological order with the apex of the Dirac cone, called Dirac Point (DP) at finite binding energies due to finite charge carrier doping arising from impurities, imperfections, etc. [8–10] These states often show instability with time and complex time evolutions [5, 6], which has been attributed to different phenomena such as relaxation of Van der Waals bond [11], the surface band bending [5], dangling surface states [12], etc. There exists contrasting arguments indicating the necessity of unusually large change in the bond length for the relaxation of Van der Waals bonds [13]. Evidently, the real materials exhibit significant deviations from theoretical wisdom [14–16] albeit the electronic states being topologically protected. Here, we discover that the behavior of the topological states is dependent on surface terminations. The anomalies in the behavior of the Dirac particles actually depends on subtle interactions of the adsorbates with the surface atoms.

In Fig. 1, we show the signature of Dirac cone representing the topological surface states in the angle resolved photoemission spectroscopic (ARPES) data. The high symmetry points and the Brillouin zone defined in the reciprocal space of Bi_2Se_3 are shown in Fig. 1(b). In addition to the metallic Dirac states, several bulk bands cross the Fermi level, ϵ_F indicating

metallicity of the bulk electronic structure [1, 2]. Curiously, the Dirac point appears at an unusually high binding energy of about 0.45 eV. To ascertain the reproducibility of these data, the sample was cleaved several times and measured in identical conditions. We discover results of two categories. (i) In one case, DP appears around 0.3 eV binding energy as shown in Fig. 2, consistent with the earlier results [1, 2, 5, 6]. We denote this case as 'Clv1'. (ii) In the other case denoted as 'Clv2', the DP appears around 0.45 eV binding energy. Time evolution of the 'Clv2' spectra at 20 K is shown in Figs. 1(c) - 1(e) and corresponding energy distribution curves (EDC) in 1(f) - 1(h). Ironically, the DP shifts towards ϵ_F with the increase in time delay from cleaving suggesting an effective hole doping with time and/or passivation of the electron doped bulk with aging.

DP in the 'Clv1' spectra shown in Fig. 2 appears around 0.3 eV for freshly cleaved surface and gradually shifts away from ϵ_F with the increase in time delay suggesting an electron doping with time. Evidently, the contrasting scenario for Clv1 and Clv2 surface is curious. DP appears to stabilize at a long time delay in both the cases. The experiments at 200 K exhibit similar trend in energy shift with a slightly different saturation value. All these results indicate that the cleaved surfaces are qualitatively different in the two cases with ϵ_F pinned at different energies and anomalous shift of the Dirac point with time. Some element specific study is necessary to reveal the surface chemistry of these materials.

We employed *x*-ray photoemission (XP) spectroscopy to probe the surface chemistry [17]. The normal emission Se 3*d* spectrum from Clv2 surface exhibits two peak structures for each spin-orbit split peaks as denoted by 'A' (54.3 eV) and 'B' (54.6 eV) in Fig. 3(a) for the 3*d*_{5/2} photoemission signal. The feature, A becomes significantly weaker in Clv1 spectra with subsequent enhancement of the feature B. The peak B enhances further in the spectra collected at 60° off-normal emission from Clv1 surface. Off-normal emission makes the technique more surface sensitive [18, 19] (the photoemission probing depth, $d = \lambda \cos\theta$, λ = escape depth and θ = emission angle with surface normal). The enhancement of B with the increase in surface sensitivity suggests its surface character, thereby, assigning the feature A to the bulk Se photoemission. Thus, the cleaving of Bi₂Se₃ leads to different surface terminations exposing Se in Clv1 case and Bi in Clv2 case. We note here that top post removal method was necessary to prepare well ordered clean sample surface exhibiting significantly strong binding between the quintuple layers.

The second important observation is shown in Fig. 3(b), where the 60° angled emission

spectra from Clv1 surface exhibit a decrease of B and subsequent increase of two weak features at higher binding energies (marked ‘SeO₂’ in the figure) indicating emergence of a new kind of Se at the cost of some of the surface Se species. The changes in the normal emission spectra from Clv2 surface, however, are not distinct indicating weak influence of aging on the subsurface Se species. The features deriving the Se 3*d* spectra were simulated by a set of asymmetric peaks as shown in Fig. 3(c). The shaded peaks represent the bulk Se photoemission and the other features correspond to the surface Se. The peak position of the emerging Se components with time and their intensity ratio indicate their origin to Se 3*d* signals from SeO₂ species[20]. Bi 4*d* spectra shown in Fig. 3(d), however, exhibit quite similar lineshape at various experimental conditions employed.

Experiments on freshly cleaved surface do not show signature of impurity features. The oxygen 1*s* signal appears to emerge with aging and gradually grows with the increase in delay time. A representative case is shown in Fig. 4(a) for Clv1 surface after normalizing by the number of scans. The Clv1 spectrum after 6 hours delay exhibits three distinct features denoted by A, B and C in Fig. 4(b). The Clv2 spectrum at about 6 hours delay exhibits relatively more intense A and weaker C with no trace of B suggesting different characteristics of adsorbed oxygens on different surfaces. In both the cases, the feature A grows quickly relative to the other features as shown in Fig. 4(c).

Now, the question is, if this surface modification influences Dirac states although they are protected by topological order. In Fig. 4(d), we show the evolution of the Dirac point with aging and observe that the DP in Clv1 spectra appears around 0.3 eV, on freshly cleaved surface. With increase in time delay, it gradually shifts towards higher binding energies with time and stabilizes around 0.4 eV. The same set of experiments at 200 K exhibit DP around 0.3 eV along with a weaker energy shift saturating around 0.38 eV that opens up new possibilities in understanding the behavior of these exotic states vis a vis existing wisdoms [16, 21, 22]. Ironically, the Clv2 spectra exhibit a reverse scenario with DP appearing at much higher binding energy of 0.45 eV and shifting in the opposite direction implying an effective hole doping case. The time evolution of DP can be expressed as,

$$\epsilon_{DP}(t) = \epsilon_0 - \alpha \times \exp(-t/t_{k1}) + \beta \times \exp(-t/t_{k2})$$

Here, ϵ_0 = DP at long delay time, t , t_{k1} and t_{k2} are the time constants. α and β are positive and are related to the electron and hole doping, respectively. The data points at

different conditions can be captured remarkably well with the above equation. Now, at $t = 0$, the binding energy at DP is $(\epsilon_0 - \alpha + \beta)$. Therefore, the shift of DP can be expressed as

$$\Delta\epsilon(t) = \alpha[1 - \exp(-t/t_{k1})] - \beta[1 - \exp(-t/t_{k2})]$$

values of ϵ_0 , α and β are 0.41, 0.13 & 0.02 for 'Clv1' at 20 K; 0.38, 0.12 & 0.02 for 'Clv1' at 200 K, and 0.35, 0.16 & 0.25 for 'Clv2' at 20 K. The parameters are quite similar in all the cases except a large β for the 'Clv2' case. t_{k1} and t_{k2} are 6 hrs and 16 hours at 20 K in both the cleaved cases. t_{k1} becomes 4 hrs at 200 K leaving t_{k2} unchanged. The growth of oxygen can be expressed as $[1 - \exp(-t/t_k)]$ with $t_k = 16$ hrs for the features B & C, and 6 hrs for A at 20 K indicating a possible link between the DP shift and oxygen growth.

Since the time delay primarily modifies the surface, the chemical potential shift must be due to the change in electron count in the surface electronic structure [23]. Three types of oxygen species are found to grow on the surface. The feature A grows quickly and have dominant contribution on Clv2 (Bi terminated) surface. The feature B is absent in Clv2 spectra and have large contribution in Clv1 spectra (Se-terminated surface) suggesting its bonding with surface Se leading to electron doping, while the feature A corresponds to oxygen bonded to Bi leading to hole doping.

The charge densities on the surface are calculated using full potential density functional theory and shown in Fig. 5. The Bi terminated surface exhibit highly extended electron density spreading over a larger spatial distance away from the surface compared to the Se-terminated case. The Fermi surface corresponding to the Bi-terminated surface is significantly larger than that corresponding to Se-terminated case. Thus, DP is expected to appear at higher binding energy in Bi-terminated case compared to the Se-terminated case as found experimentally.

Se and O belong to the same group of the Periodic table with O being the topmost element with higher electronegativity. Therefore, O on Se surface forms SeO_x complex (signature of SeO_2 appears in the Se 3d spectra). Se-O bonding will attract electron cloud from the neighborhood reducing the electron density in the Bi-Se neighborhoods as manifested in the left panel of Fig. 5 by increase in spatial charge density contours around oxygen sites relative to the pristine case. Since the conduction band consists of p electrons, this would lead to an effective electron doping in the conduction band. On the other hand, oxygen on Bi-terminated surface would form BiO_x complexes leading to more charge localization in the

vicinity of oxygens (see right most panel of Fig. 5) reducing the Fermi surface volume; an effective hole doping scenario.

In summary, we studied the surface electronic structure of a topological insulator, Bi_2Se_3 employing high resolution photoemission spectroscopy. We observe the sensitivity of the Dirac states on surface termination. The surface states and the impurities appear to play a complex role leading to complex Fermi surface reconstructions emerging as a shift of the Dirac cone. These materials have been drawing much attention due to their potential technological applications in addition to the fundamental issues of realizing magnetic monopoles, the observation of Majorana fermions, etc. The results presented here reveal the complex microscopic details of the surface states necessary in the realization of such ambitious projects in real materials.

METHOD

High quality single crystals of Bi_2Se_3 were prepared by Bridgeman method and characterized using x -ray Laue diffraction. Angle resolved photoemission (ARPES) measurements were carried out employing Gamdata Scienta R4000WAL electron analyzer, monochromatic laboratory sources and an open cycle helium cryostat. The energy and angle resolution were set to 10 meV and 0.1° to have adequate signal to noise ratio without compromising the resolution necessary for this study. The sample was cleaved several times *in situ* at the experimental temperature using a top post glued on top of the sample. The well ordered sample surface has been verified by bright sharp low energy electron diffraction spots. X -ray photoemission spectra from freshly cleaved sample was found clean with no oxygen or carbon related signals.

The electronic band structure of a slab of Bi_2Se_3 was calculated employing *state of the art* full potential linearized augmented plane wave method using Wien2k software[24]. The bulk electronic structure exhibits a gap consistent with its insulating behavior [25, 26] and the results from slab calculations show signature of Dirac cone in the presence of spin-orbit coupling.

ACKNOWLEDGEMENTS

K. M. acknowledges financial support from the Dept. of Science and Technology, Govt. of India under the ‘Swarnajayanti Fellowship programme’, the Dept. of Atomic Energy, Govt. of India, and the Alexander von Humboldt Foundation, Germany. G. B. wishes to thank EPSRC, UK for financial support through Grant EP/I007210/1.

-
- [1] Hasan, M. Z. & Kane, C. L. Topological insulators. *Rev. Mod. Phys.* **82**, 3045 (2010).
 - [2] Fu, L., Kane, C. L. & Mele, E. J. Topological Insulators in Three Dimensions. *Phys. Rev. Letts.* **98**, 106803 (2007).
 - [3] Fu, L. & Kane, C. Superconducting Proximity Effect and Majorana Fermions at the Surface of a Topological Insulator. *Phys. Rev. Letts.* **100**, 096407 (2008).
 - [4] Qi, X.-L., Li, R., Zang, J. & Zhang, S.-C. Inducing a Magnetic Monopole with Topological Surface States. *Science* **323**, 1184-1187 (2009).
 - [5] Hsieh, D. et al. A tunable topological insulator in the spin helical Dirac transport regime. *Nature* **460**, 1101-1105 (2009).
 - [6] Kong, D. et al. Rapid Surface Oxidation as a Source of Surface Degradation Factor for Bi₂Se₃. *ACS Nano* **5**, 46984703 (2011).
 - [7] Reis, D. D. et al., Surface structure of Bi₂Se₃(111) determined by low-energy electron diffraction and surface x-ray diffraction. *Phys. Rev. B* **88**, 041404(R) (2013).
 - [8] Yashina, L. V. et al. Negligible Surface Reactivity of Topological Insulators Bi₂Se₃ and Bi₂Te₃ towards Oxygen and Water. *ACS Nano* **7**, 5181 (2013).
 - [9] Atuchin, V. V. et al. Formation of Inert Bi₂Se₃(0001) Cleaved Surface. *Crystal Growth & Design* **11**, 55075514 (2011).
 - [10] Golyashov, V. A. et al. Inertness and degradation of (0001) surface of Bi₂Se₃ topological insulator. *J. Appl. Phys.* **112**, 113702 (2012).
 - [11] Noh, H.-J. et al. Spin-orbit interaction effect in the electronic structure of Bi₂Te₃ observed by angle-resolved photoemission spectroscopy. *Europhys. Letts.* **81**, 57006 (2008).
 - [12] Lin Hsin et al. Topological Dangling Bonds with Large Spin Splitting and Enhanced Spin Polarization on the Surfaces of Bi₂Se₃. *Nano Lett.* **13**, 1915-1919 (2013).

- [13] Fukui, N. *et al.* Surface relaxation of topological insulators: Influence on the electronic structure. *Phys. Rev. B* **85**, 115426 (2012).
- [14] Bianchi, M. *et al.* Coexistence of the topological state and a two-dimensional electron gas on the surface of Bi_2Se_3 . *Nat. Commun.* **1**, 128 (2010).
- [15] Wang, X., Bian, G., Miller, T. & Chiang, T.-C. Fragility of Surface States and Robustness of Topological Order in Bi_2Se_3 against Oxidation. *Phys. Rev. Letts.* **108**, 096404 (2012).
- [16] Zhang, Z. & Yates Jr. J. T., Band Bending in Semiconductors: Chemical and Physical Consequences at Surfaces and Interfaces. *Chem. Rev.* **112**, 5520 (2012).
- [17] Maiti, K. *et al.* Doping dependence of the chemical potential and surface electronic structure in $\text{YBa}_2\text{Cu}_3\text{O}_{6+x}$ and $\text{La}_{2-x}\text{Sr}_x\text{CuO}_4$ using hard x-ray photoemission spectroscopy, *Phys. Rev. B* **80**, 165132 (2009).
- [18] Maiti, K. *et al.*, Understanding the bulk electronic structure of $\text{Ca}_{1-x}\text{Sr}_x\text{VO}_3$. *Phys. Rev. B* **73**, 052508 (2006);
- [19] Singh, R. S. *et al.*, Evidence for strong $5d$ electron correlations in the pyrochlore $\text{Y}_2\text{Ir}_2\text{O}_7$ studied using high-resolution photoemission spectroscopy. *Phys. Rev. B* **77**, 201102(R) (2008).
- [20] Kont, D. *et al.* Rapid Surface Oxidation as a Source of Surface Degradation Factor for Bi_2Se_3 . *ACS Nano* **5**, 46984703 (2011).
- [21] Benia, H. M., Lin, C., Kern, K. & Ast, C. R. Reactive Chemical Doping of the Bi_2Se_3 Topological Insulator. *Phys. Rev. Letts.* **107**, 177602 (2011).
- [22] Bianchi, M., Hatch, R. C., Mi, J., Iversen, B. B. & Hofmann, P. Simultaneous Quantization of Bulk Conduction and Valence States through Adsorption of Nonmagnetic Impurities on Bi_2Se_3 . *Phys. Rev. Letts.* **107**, 086802 (2011).
- [23] Maiti, K., Medicherla, V. R. R., Patil, S., & Singh, R. S. Revelation of the role of impurities and conduction electron density in the high resolution photoemission study of ferromagnetic hexaborides. *Phys. Rev. Lett.* **99**, 266401 (2007).
- [24] Blaha, P., Schwarz, K., Madsen, G. K. H., Kvasnicka, D. & Luitz, J. [WIEN2k An Augmented Plane Wave + Local Orbitals Program for Calculating Crystal Properties.] [Schwarz, K. (ed.)] (Techn. Universität Wien, Austria, 2001).
- [25] Larson, P., Greanya, V. A., Tonjes, W. C., Liu, R. & Mahanti, S. D. Electronic structure of Bi_2X_3 ($\text{X}=\text{S}, \text{Se}, \text{T}$) compounds: Comparison of theoretical calculations with photoemission studies. *Phys. Rev. B* **65**, 085108 (2002).

- [26] Mishra, S. K., Satpathy, S. & Jepsen, O. Electronic structure and thermoelectric properties of bismuth telluride and bismuth selenide. *J. Phys. Condens. Matter* **9**, 461-470 (1997).

AUTHOR CONTRIBUTIONS

D. B. and S. T. carried out the photoemission measurements. D. B. carried out band structure calculations and helped in data analysis. K. A. helped in the experiments. G. B. prepared the sample and characterized them. K. M. initiated the study, supervised the measurements, analyzed the data, prepared the figures & the manuscript.

COMPETING FINANCIAL INTERESTS

The authors declare no competing financial interests.

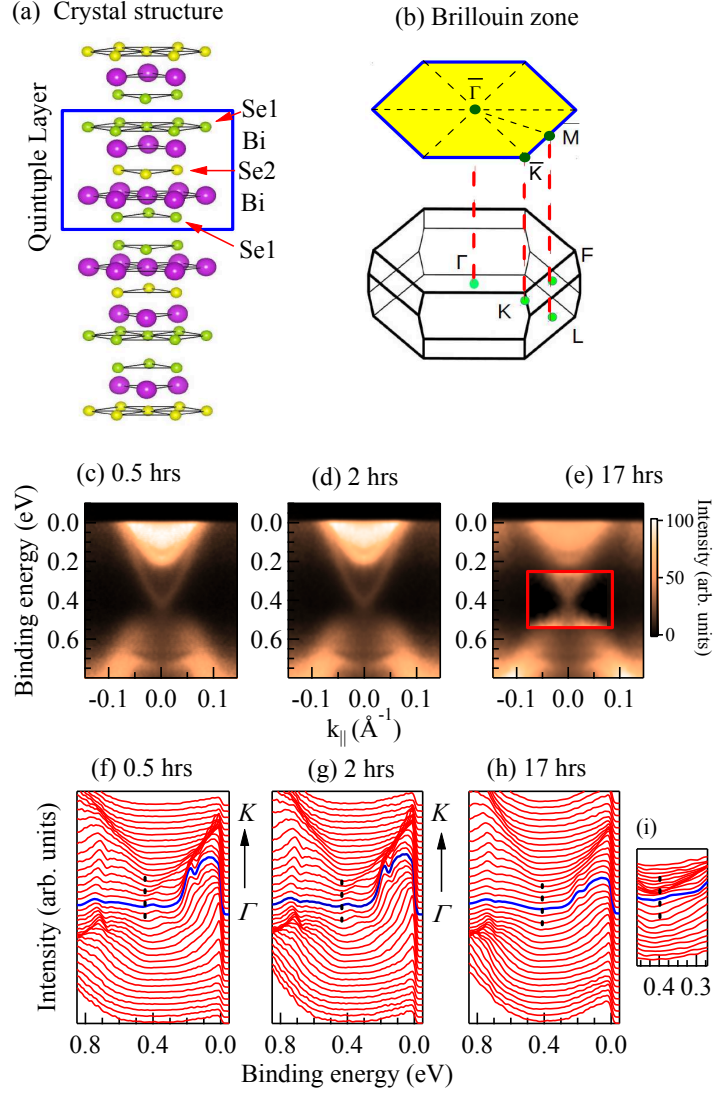


FIG. 1. (a) Crystal structure of Bi_2Se_3 exhibiting stack of quintuple layers of Bi and Se and corresponding (b) Brillouin zone. ARPES data at 20 K along $\Gamma - K$ for 'Clv2' after (c) 0.5 hrs, (d) 2 hrs and (e) 17 hours of cleaving. (f) - (g) show the corresponding energy density curves. (i) Rescaled spectral region exhibiting the Dirac point with better clarity.

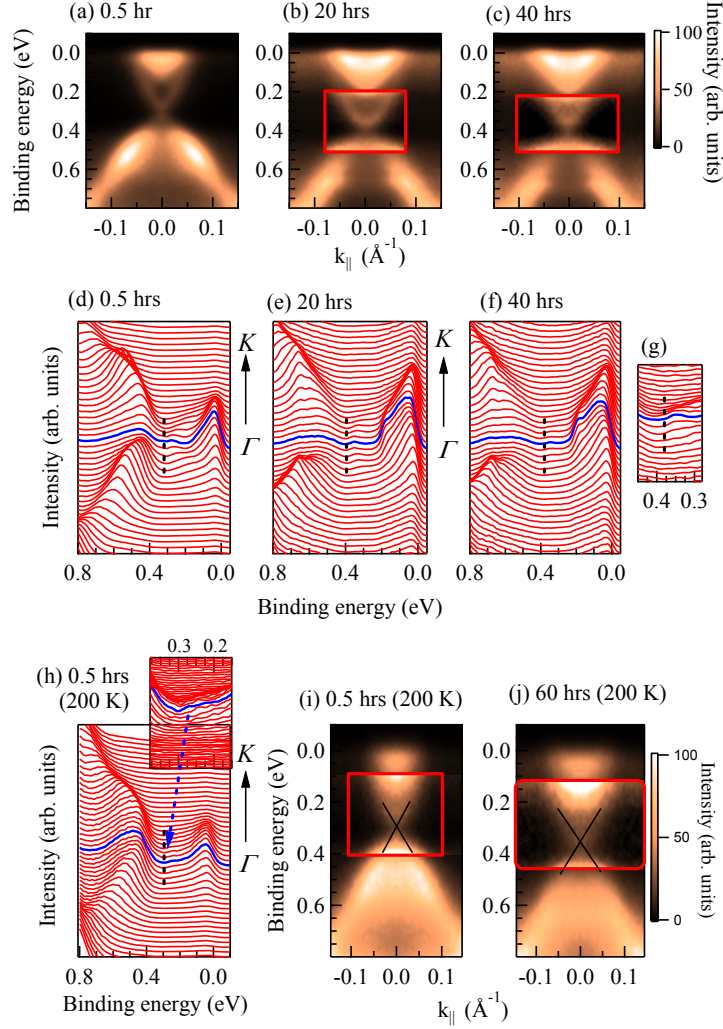


FIG. 2. (a) ARPES data at 20 K along $\Gamma - K$ direction from Clv1 surface after (a) 0.5 hrs, (b) 20 hrs and (c) 40 hours after cleaving. (d) - (f) show the corresponding energy density curves. (g) Rescaled spectral region near Dirac point. (h) EDC at 200 K. ARPES data at 200 K at (i) 0.5 hrs and (j) 60 hours after cleaving.

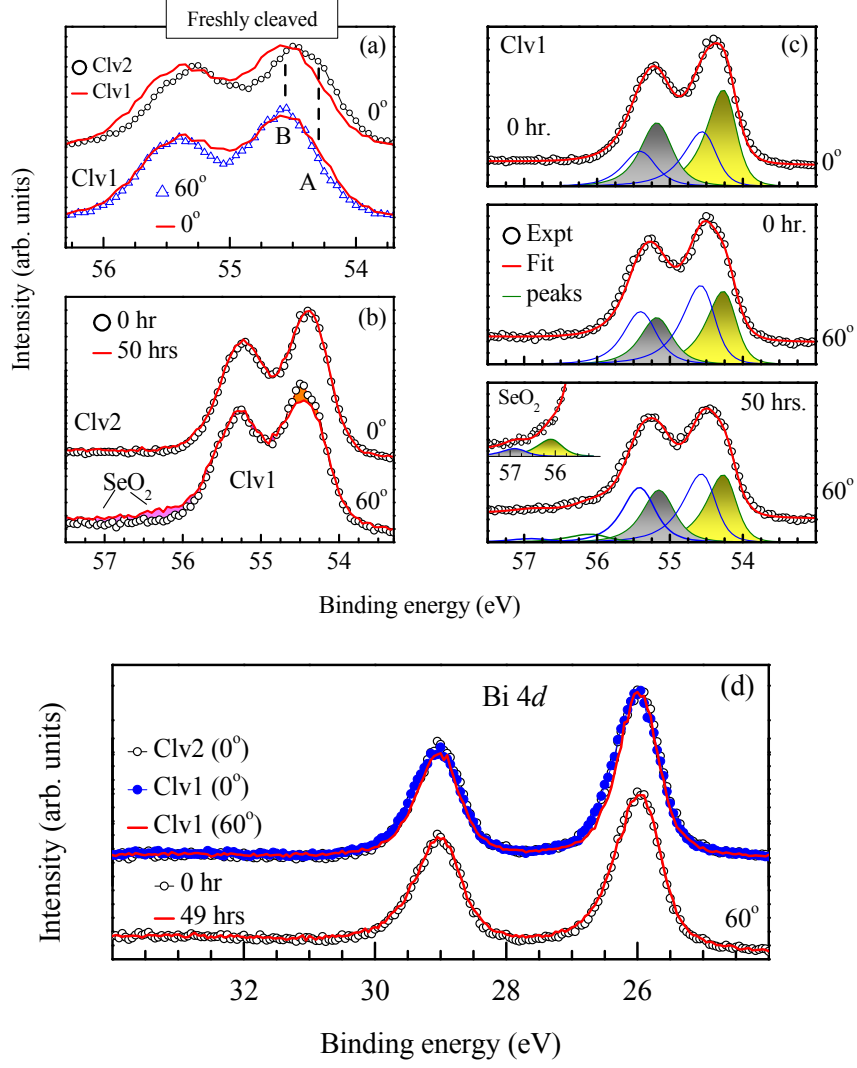


FIG. 3. (a) Se 3d spectra from Clv1 (line) and Clv2 (open circles) surfaces at normal emission. The open triangles are the Clv1 data at 60° off-normal electron emission. (b) Se 3d spectra at normal emission from Clv2 surface and at 60° off-normal emission from 'Clv1' surface. The data from freshly cleaved surface and after 50 hours of delay are shown by lines and open circles, respectively. (c) The fit of the Se 3d spectra from Clv1 at different emission angles and time delay. (d) Bi 4d spectra from Clv1 and Clv2 surfaces at different emission angles and delay times exhibiting identical lineshape for every case.

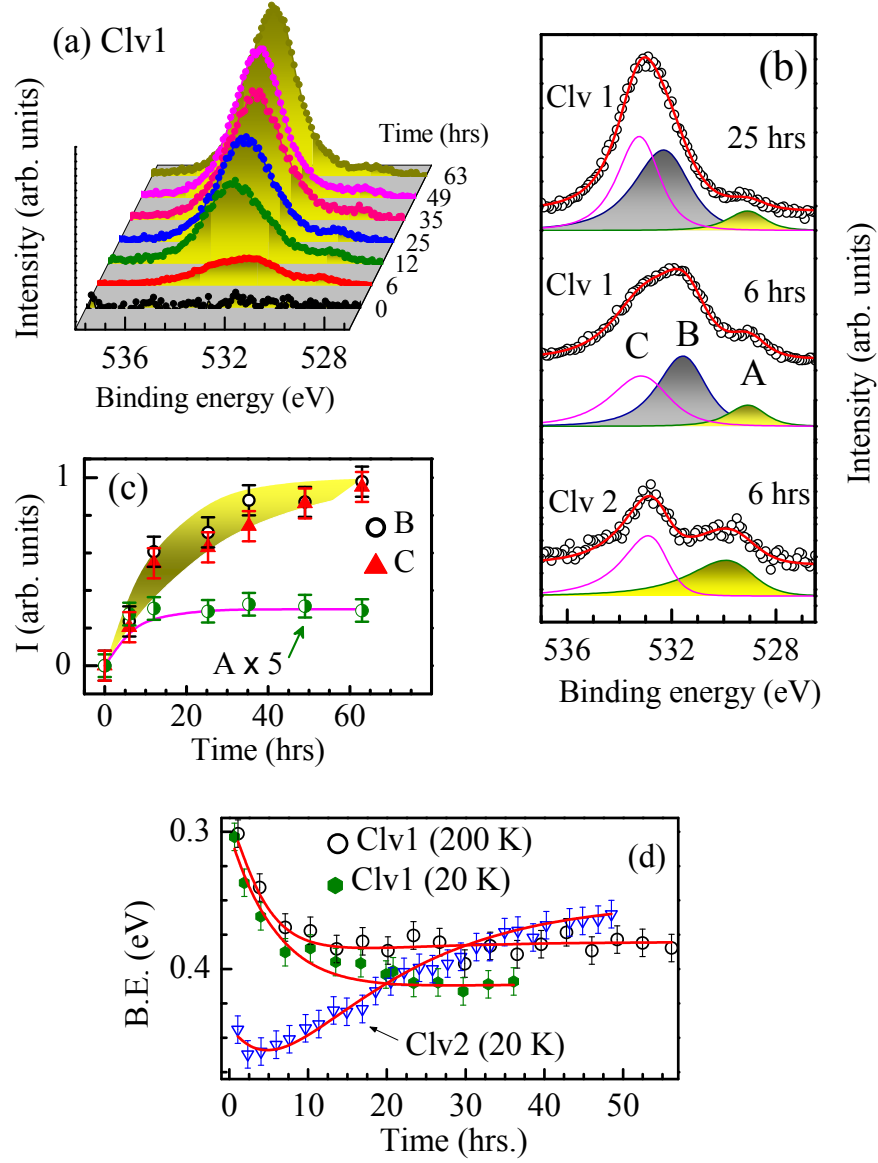


FIG. 4. (a) Growth of O 1s feature on Clv1 surface with time at 20 K. (b) Fit of the O 1s spectra from both Clv1 and Clv2 surfaces with asymmetric peaks. Except the feature A, all the features of 25 hrs delay spectrum are compressed by 2 times for clarity. (c) Evolution of the O 1s intensities with time. The line and the shaded region show exponential time dependence. (d) Binding energy shift of the Dirac point with time (symbols). The lines show exponential fits.

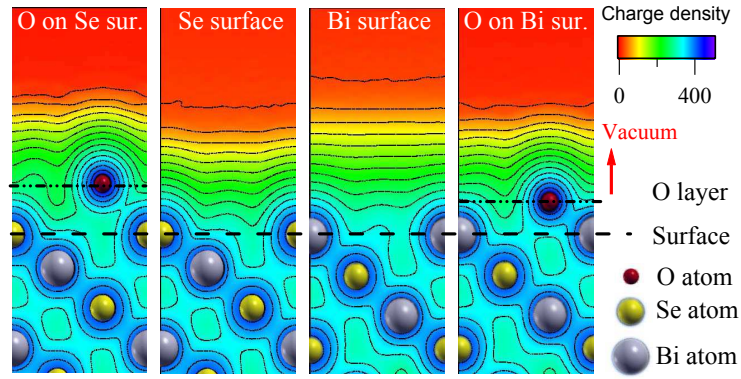


FIG. 5. Calculated charge density plots (left to right) for oxygen on Se-terminated surface, Se terminated surface, Bi terminated surface and oxygen on Bi-terminated surface.